

SUPPLEMENTARY INFORMATION

for

“Chromatin decouples promoter threshold from dynamic range”

Felix H. Lam, David J. Steger, Erin K. O’Shea *

* To whom correspondence should be addressed. E-mail: erin_oshea@harvard.edu

This pdf file includes:

Materials and Methods

| | |
|--|-----|
| Yeast strains | S3 |
| Media and growth conditions..... | S5 |
| Phosphate-free modified synthetic complete medium..... | S6 |
| Steady-state dose response measurements..... | S7 |
| Kinetics of induction..... | S8 |
| Nucleosome maps | S8 |
| Identification of Pho4 motifs | S11 |
| Pho4 position-specific scoring matrix | S12 |
| Pho4 chromatin immunoprecipitation (ChIP)..... | S13 |
| Flow cytometry analysis | S16 |
| Descriptive statistics and expression variability..... | S18 |

Discussion

| | |
|---|-----|
| Feedback effects..... | S21 |
| Resolvability of individual Pho4 sites by ChIP | S21 |
| Resolvability of individual Pho4 sites by ChIP simulation | S22 |
| Dynamic range of <i>PHO</i> genes | S24 |
| Prediction of expression in YPD..... | S25 |

| | |
|-----------------|-----|
| References..... | S26 |
|-----------------|-----|

Supplementary Figures S1-S10

Supplementary Tables S1-S7

Materials and Methods

Yeast strains. Haploid transcriptional reporter strains (Supplementary Table S4) containing variants of the *PHO5* promoter were constructed via the pop-in/pop-out gene replacement method¹. Briefly, a series of pRS306-based plasmids containing a portion of the *PHO5* coding sequence and our desired promoter mutations was created by oligonucleotide-directed mutagenesis, linearized by PflMI, and integrated (pop-in) at the native *PHO5* locus in EY57 (K699 *MATa ade2-1 trp1-1 can1-100 leu2-3,112 his3-11,15 ura3*) cells. Subsequent elimination of the marker in uracil prototrophs was accomplished by selecting for uracil auxotrophy (pop-out) through growth on synthetic medium containing 5-fluoroorotic acid^{2,3}. The ectopic high affinity Pho4 motif located within the central nucleosome -3 region was introduced at position -481 through three base substitutions (cttatgtgcgc to ct**CaCgtgGgc**). Mutations swapping affinity at either of the two native Pho4 binding site locations (-362, -253) were done through two base substitutions: ag**cacgttttc** to ag**cacgtGGtc** (low to high affinity), or **cacacgtggga** to **cacacgtTTga** (high to low affinity). Ablations of either site were achieved through conversion of the core 6 bp CACGT(G|T) motif to a HindIII site (AAGCTT). The presence of a successfully introduced or swapped high affinity Pho4 site could be followed by PCR and digestion with PmlI. Mutations neither inserted nor deleted nucleotides in order to conserve the total promoter length, and were ultimately confirmed by DNA sequencing of the genomic *PHO5* locus.

After creation of the various promoter mutants, substitution of the *PHO5* protein coding sequence with the yeast-enhanced green fluorescent protein (yeGFP1) reporter was performed through PCR-mediated direct gene replacement⁴. A 0.7 kb PacI/AscI fragment containing

yeGFP1 was liberated from plasmid EB1631 and ligated into PacI/AscI-digested pFA6a-GFP(S65T)-kanMX6, thus replacing GFP(S65T) with yeGFP1⁵. The resulting plasmid (EB1632) was used with primers containing *PHO5* targeting sequences (Supplementary Table S6) and an optimized translation initiation signal directly preceding the start codon to generate a 2.4 kb PCR product containing the yeGFP1-kanMX6 gene replacement cassette⁶. Material from eight to ten PCR reactions was pooled, concentrated and purified through the QIAquick PCR Purification Kit (QIAGEN #28106, www.qiagen.com), and used to transform *S. cerevisiae* strains containing the *PHO5* promoter mutations. Transformed cells were allowed to recover overnight at 30°C on YPD plates before replica-plating to YPD plates containing 200 µg/ml G418. Stably integrated, G418-resistant transformants appeared approximately after 48 hrs of growth, and candidates were validated both functionally by induction in P_i starvation (0 µM P_i) medium and flow cytometry, and by PCR using primers specific to the *PHO5* promoter and yeGFP1 coding sequence.

Constitutively-activated versions of the *PHO5* promoter variants approximating expression in P_i starvation were created by deletion of the *PHO80* gene which results in unphosphorylatable, constitutively active Pho4⁷. In lieu of direct gene replacement via transformation, we mated our series of *PHO5* promoter variants to EY135 (K699 *MATα ade2-1 trp1-1 can1-100 leu2-3,112 his3-11,15 ura3, pho80Δ::CgHIS3*), sporulated diploids, and dissected tetrads to isolate haploids exhibiting both G418 resistance and histidine prototrophy.

Heterozygous diploid transcriptional reporter strains (Supplementary Table S5), with the exception of EY2230 and EY2231, were created in a manner similar to the haploid transcriptional reporter strains described above. Briefly, primers containing an idealized Kozak

element and gene-specific targeting sequences (Supplementary Table S6) were used with plasmid template EB1632 to produce yeGFP1-kanMX6 gene replacement cassettes.

Concentrated and purified PCR products were used to transform EY2176 and EY2177 diploid strains. G418-resistant candidates were validated by PCR for both the yeGFP1 and native coding alleles, and by induction in P_i starvation medium and flow cytometry.

The diploid transcriptional reporter strain EY2230 was created by mating EY1995 (K699 *MAT α ade2-1 trp1-1 can1-100 leu2-3,112 his3-11,15 ura3::PHO84pr-yeGFP1-URA3*) to EY91 (K699 *MAT α ade2-1 trp1-1 can1-100 leu2-3,112 his3-11,15 ura3*). Strain EY2231 was created through a series of matings: first by EY1995 to EY135 and double uracil/histidine selection to create EY1998 (K699 *MAT α ade2-1 trp1-1 can1-100 leu2-3,112 his3-11,15 ura3::PHO84pr-yeGFP1-URA3 pho80 Δ ::CgHIS3*), and finally by EY1998 to EY135 to yield the homozygous *pho80 Δ* transcriptional reporter. Thus, both EY2230 and EY2231 maintain two functional copies of *PHO84*.

Media and growth conditions. Yeast strains were cultured at 30°C in synthetic complete medium containing 2% glucose and supplemented to final concentrations of 0.13 mg/ml adenine and 0.1 mg/ml tryptophan (modified Difco Yeast Nitrogen Base, see below) to suppress autofluorescence. Media stocks with varying amounts of extracellular P_i were prepared from a phosphate-free base containing the above, and supplemented with monobasic potassium phosphate to the following final concentrations: 10 μ M, 50 μ M, 100 μ M, 500 μ M, 1 mM, 5 mM, 10 mM, and 50 mM. All media stocks were adjusted to pH 4 with HCl⁸.

Phosphate-free modified synthetic complete medium (per L)⁹

Nitrogen Source

5 g Ammonium sulfate

Carbon Source

20 g Dextrose

Amino Acids

130 mg Adenine sulfate
20 mg L-Arginine
20 mg L-Histidine
30 mg L-Isoleucine
100 mg L-Leucine
30 mg L-Lysine
20 mg L-Methionine
50 mg L-Phenylalanine
200 mg L-Threonine
100 mg L-Tryptophan
30 mg L-Tyrosine
20 mg Uracil
150 mg L-Valine

Vitamins

2 µg Biotin
400 µg Calcium pantothenate
2 µg Folic acid
2 mg Inositol
400 µg Niacin
200 µg *p*-Aminobenzoic acid
400 µg Pyridoxine hydrochloride
200 µg Riboflavin
400 µg Thiamine hydrochloride

Trace Elements

500 µg Boric acid
40 µg Copper sulfate
100 µg Potassium iodide
200 µg Ferric chloride
400 µg Manganese sulfate
200 µg Sodium molybdate
400 µg Zinc sulfate

Salts

1.5 g Potassium chloride (in lieu of monopotassium phosphate)
0.5 g Magnesium sulfate
0.1 g Sodium chloride
0.1 g Calcium chloride

Steady-state dose response measurements. Based on pilot measurements of *PHO* pathway induction in 10 μM P_i conditions, we estimated the minimum time to reach steady-state fluorescence to be approximately 16 hrs whereby median expression changes less than 5% per hour (data not shown). We therefore selected 18 hr as an appropriate time point representing steady-state. To avoid significant P_i depletion from intermediate P_i (10-500 μM) media over the course of growth to steady-state expression, we calculated inoculum volumes such that the final cell density at the end of 18 hrs would be 5×10^4 cells/ml. Based on a measured phosphate uptake rate of 12.37×10^{-9} mol P_i min^{-1} OD_{600}^{-1} , we calculated that less than 10 nmol P_i is depleted in the duration of such an experiment¹⁰. Haploid strains growing in synthetic medium were estimated to have doubling times of ~ 110 min, and diploids ~ 100 min. These times were observed to be robust even in media containing as low as 10 μM P_i (data not shown).

Transcriptional reporter strains maintained on synthetic complete (high P_i) plates were inoculated into 10 mM P_i liquid medium and maintained in exponential growth for a minimum of 9 hrs to ensure repression of the *PHO* pathway. For measurement samples, the starter culture was diluted into medium lacking P_i to minimize P_i spillover and immediately used to inoculate tubes containing 0-50 mM P_i media pre-warmed to 30°C. After 18 hr of growth, cells were placed on ice and sonicated for 3 s at 20% power before flow cytometry.

For measurements of gene expression in a *pho80* Δ genetic background (Fig. 3), strains were prepared similarly and grown in 10 mM P_i medium for 18 hrs to a final cell density of OD 0.05-0.1.

For measurements of expression in YPD (Supplementary Fig. S10), starter cultures of diploid transcriptional reporter strains were maintained in exponential growth in YPD for a

minimum of 9 hrs before seeding measurement cultures. Similarly, inoculum volumes were calculated to target a cell density of 5×10^4 cells/ml after 18 hr of growth using a cell cycle of ~80 min; for strains in a homozygous *pho80* Δ genetic background, we used a doubling time of ~90 min.

A wild-type strain without yeGFP1 grown in the appropriate medium was included in all experiments for measuring autofluorescence.

Kinetics of induction. Starter cultures of transcriptional reporter strains were grown overnight in 10 mM P_i to early/mid-logarithmic phase in order to ensure repression of the *PHO* pathway. Approximately 0.2-0.3 OD units of cells were harvested, washed twice in no P_i medium pre-warmed to 30°C, and finally resuspended in pre-warmed medium lacking P_i at a cell density of OD 0.01-0.05. Aliquots taken every 15-20 min over 7 hrs were placed on ice and sonicated for 3 s at 20% power before flow cytometry. A wild-type strain without yeGFP1 grown in 10 mM P_i was included for measuring autofluorescence. For comparison across strains, the median expression at each time point was scaled to the medians at 0 hrs and 7 hrs (minimum and maximum, respectively).

Nucleosome maps (adapted from techniques previously described¹¹⁻¹³). Nucleosome positions for the *PHO* promoters were assayed in the haploid wild-type *PHO5* transcriptional reporter strain EY1903 (Fig. 2a,b; Supplementary Fig. S6) or in *pho2* Δ strain EY2387 (K699 *MATa ade2-1 trp1-1 can1-100 leu2-3,112 his3-11,15 ura3, pho2* Δ ::*CgHIS3*; Supplementary Fig. S7), as indicated. For Supplementary Fig. S2, the appropriate *PHO5* promoter variant strain (listed in

Supplementary Table S4) was used. Approximately 100-125 OD units of mid-log cultures grown overnight in 10 mM P_i medium (“high P_i”), or subsequently induced for 2 hrs in 100 μM P_i medium (“intermediate P_i”) or 4.5 hrs in P_i starvation medium (“no P_i”) were harvested, treated with lyticase to produce spheroplasts, divided into multiple samples, and digested with 0.5-2 U of micrococcal nuclease (Sigma-Aldrich #N5386, www.sigmaaldrich.com) for 15-30 min at 37°C. The reaction was stopped and spheroplasts lysed by the addition of 25 mM EDTA and 0.5% SDS, and further treated with 0.5 mg/ml proteinase K for 2-3 hrs at 37°C before DNA purification by phenol/chloroform extraction and ethanol precipitation. Samples were subsequently treated with RNase A (0.1 mg/ml) before analysis by agarose gel electrophoresis (Supplementary Fig. S1a). Mononucleosome-length DNA fragments were gel-extracted using the QIAquick Gel Extraction Kit (QIAGEN #28706, www.qiagen.com) and further diluted 10-fold for use as template in quantitative PCR (Q-PCR).

Primer pairs tiling the length of a promoter region (~1 kb upstream of translation start) were designed using Primer3 to yield 95-105 bp products centered every 25-60 bp¹⁴ (Supplementary Fig. S1b). The position at the center of the PCR products is used as the abscissa value for points plotted in the promoter chromatin maps (Figs. 2a,b; Supplementary Fig. S2, S6 and S7). Quantification was conducted on an Mx3000P (Stratagene, www.stratagene.com) Q-PCR system through real-time fluorescence detection of SYBR Green I (Sigma-Aldrich #S-7567, www.sigmaaldrich.com). A dilution series of EY1903 genomic DNA was used to establish standard curves specific to each primer pair. In general, R^2 values from linear regression exceeded 0.995, and the range was sufficiently large to avoid extrapolation. The data from any

primer pairs found to yield heterogeneous PCR products (as assessed through melting curve analysis) were discarded.

Each 96 well plate included a primer pair targeting the heterochromatic *REC104* locus as a normalization control for plate-to-plate variation and for comparison of nucleosome positions between different P_i conditions within a single promoter and genetic background. To generate the “normalized Q-PCR” plots of Fig. 2a,b and Supplementary Fig. S6 and S7, we normalized again to the tallest peak within the promoter, typically found in high P_i . For example, for each promoter in Supplementary Fig. S6, the high (black circles), intermediate (dashed squares), and no P_i (dotted diamonds) traces assayed from wild-type cells are all normalized to the largest PCR signal which was found in high P_i . Correspondingly, for nucleosome positions assayed in *pho2Δ* cells (Supplementary Fig. S7), the high (blue circles) and no P_i (dotted diamonds) traces are normalized to the tallest peak found among these two conditions. While peak heights progressively decrease from high to no P_i and is consistent with increasing induction and degrees of chromatin remodeling, we have not rigorously established the linearity between nucleosome occupancy and protection from micrococcal nuclease. We have therefore limited the interpretation of this data mainly to the deduction of nucleosome positions and hence, location of accessible Pho4 motifs. We emphasize that peaks heights should mainly be viewed qualitatively.

As stated above, peaks of PCR signal represent enrichment of DNA segments protected by nucleosomes from micrococcal nuclease digestion, and valleys represent nucleosome-free segments (Supplementary Fig. S1c). Because these are population measurements, differences in peak heights within a promoter could reflect either heterogeneous protection from digestion across a population or differential nucleosome stability (e.g., fractional occupancy). Indeed, the

single-promoter methylase protection measurements made by Jessen *et al.*, (2006) at *PHO5* in high P_i and *pho4* Δ conditions suggest a combination of both influences¹⁵.

The relatively un-remodeled chromatin of *PHM2* and *PHM4* in P_i starvation (Supplementary Fig. S6b) is not artifactual as nucleosome maps of induced promoters were all assayed from a single micrococcal nuclease-treated sample. It is possible that the lack of nucleosome displacement is correlated with the absence of inaccessible Pho4 binding sites and confers a slight advantage in induction kinetics among *PHO* target genes (Fig. 2d).

Identification of Pho4 motifs. Previous studies in *S. cerevisiae* have tabulated the presence of two Pho4 consensus sequences (CACGTG vs. CACGTT) among P_i -regulated genes^{16,17}.

However, to identify Pho4 motifs among our selection of *PHO* promoters in a more systematic fashion, we employed a basic informatics discovery approach using a position-specific scoring matrix (PSSM) generated from the Pho4 binding affinities measured by Maerkl and Quake¹⁸. From the 256 $\Delta\Delta G_{full}$ values determined using Pho4 and the NNNNGTG DNA oligomer library, we computed the corresponding probabilities of binding assuming a temperature of 298 K, and produced an initial PSSM for the E-box 5' half-site and flanking base (i.e., permuted positions only). To reflect the homodimeric nature of Pho4 binding to DNA¹⁹ and the optimality of palindromic motifs¹⁸, we extended the PSSM to accommodate a full octameric sequence by reverse-complementing the base probabilities to fill the 3' half-site plus flanking position. Pseudocounts were added to correct for finite sampling and measurement error, and the resulting renormalized PSSM used to scan our selection of *PHO* promoters for potential Pho4 binding sites²⁰.

Pho4 position-specific scoring matrix

| A | C | G | T |
|--------------------|--------------------|--------------------|--------------------|
| 0.244786799936867 | 0.255007630632078 | 0.374397609219465 | 0.12580796021159 |
| 0.119955498380329 | 0.759356790557335 | 0.0655475347868927 | 0.0551401762754437 |
| 0.772445717403354 | 0.0509075140717383 | 0.117959154592486 | 0.0586876139324211 |
| 0.0416267852229891 | 0.844114600835618 | 0.060177824315804 | 0.0540807896255892 |
| 0.0540807896255892 | 0.060177824315804 | 0.844114600835618 | 0.0416267852229891 |
| 0.0586876139324211 | 0.117959154592486 | 0.0509075140717383 | 0.772445717403354 |
| 0.0551401762754437 | 0.0655475347868927 | 0.759356790557335 | 0.119955498380329 |
| 0.12580796021159 | 0.374397609219465 | 0.255007630632078 | 0.244786799936867 |

Based on the binding profiles of *PHO5*, *PHO84*, and *PHO8* (Supplementary Fig. S4a, S4d, and S4e, respectively), whose Pho4-promoter interactions have been characterized by *in vitro* DNase I protection assays^{17,21-23}, we selected 3×10^{-4} as the probability threshold for a likely Pho4 regulatory element. Specifically, the weakest binding probability matching an experimentally-verified *in vitro* Pho4 footprint comes from *PHO8*, where the UASp1 motif at -731 gives a probability of 2.7×10^{-4} . Since this binding site was subsequently determined to be non-functional *in vivo*²⁴, we selected 3×10^{-4} as the boundary between noise and potential Pho4 motifs.

To further distinguish low from high affinity Pho4 motifs, we deferred to *in vitro* competition footprinting experiments from the literature where differences in binding affinity have been measured between *PHO5* UASp1 vs. UASp2, and *PHO84* Site D vs. Site E^{17,23}. From the binding profiles of these two promoters, the high affinity motifs — *PHO5* UASp2 and *PHO84* Site D — give probabilities of 7.7×10^{-3} and 1.2×10^{-2} , respectively. We therefore selected 7.5×10^{-3} as the most stringent probability necessary to recapitulate validated high affinity sites.

After identifying high vs. low affinity sites from the binding profiles of our representative set of *PHO* promoters (Supplementary Fig. S4), we examined how robust our affinity assignments are to the chosen threshold value. Again deferring to competition footprinting data^{17,21-23}, the validated low affinity motifs — *PHO5* UASp1 and *PHO84* Site E — both give binding probabilities of 1.8×10^{-3} . Based on this value, we determined that the threshold can be reduced almost four fold to 1.9×10^{-3} — a probability just above the validated low affinity sites — without significantly impacting our affinity assignments. The only binding site whose affinity designation changes is the initially low affinity motif at -563 in the *PHM6* promoter, a site that is nucleosomal and thus, inconsequential to induction threshold. That this reduction in motif stringency is possible without greatly affecting *in vivo* binding predictions suggests that, at least based on *in vitro* affinity characteristics, Pho4-promoter interactions may indeed be bimodal and fall robustly into two broad affinity classes.

Finally, putative Pho4 sites were plotted on multiple alignments of *Saccharomyces* orthologs using the UCSC Genome Browser (genome.ucsc.edu) to assess evolutionary conservation and likelihood of function (Supplementary Fig. S5)^{25,26}. Both conserved (red triangles, dark blue ovals) and non-conserved (light blue ovals) motifs are indicated in Fig. 2a,b and Supplementary Fig. S6-S9. The Pho4 sites identified through this approach are consistent with the Pho4-DNA interaction data available for those *PHO* promoters where binding assays have been done^{24,27}.

Pho4 chromatin immunoprecipitation (ChIP) (based on techniques previously described²⁸). Approximately 96 OD units of cells (EY57 for wild-type *PHO* promoters, EY1573 for the H4

PHO5 promoter variant) grown overnight in 10 mM P_i medium to early-log phase were harvested, divided equally into three, and used to inoculate high (10 mM P_i), intermediate (100 μ M P_i), and no P_i (0 μ M) induction cultures. A large culture volume (650 ml) was used for the intermediate P_i sample to minimize P_i depletion in the time course of induction. Based on previously published Pho4 ChIP conditions²⁹ and the nuclear localization kinetics of Pho4⁸, we induced all samples for 2.5 hrs, crosslinked in 1% formaldehyde for 15 min at room temperature, and quenched with 125 mM glycine for a minimum of 5 min. Cells were washed immediately with cold phosphate-buffered saline (PBS), and mechanically lysed with glass beads in buffer (50 mM HEPES/NaOH, pH 7.5; 140 mM NaCl; 1 mM EDTA; 1% Triton X-100; 0.1% Na-Deoxycholate) containing protease inhibitors (Roche #04-693-132-001, www.roche-applied-science.com). DNA fragments in crude whole-cell extract were further sheared to an average length of 500 bp (data not shown) by multiple cycles of sonication (5 \times 15 s pulses at 15% power). Specific chromatin fragments were subsequently immunoprecipitated from lysate using a Pho4 polyclonal antibody and protein A-sepharose beads. Protein-DNA crosslinks in both the washed immunoprecipitate (IP) and a whole-cell lysate sample (input) were selectively reversed by incubating 6 hr to overnight at 65°C in 10 mM Tris-HCl, pH 8; 1 mM EDTA; 0.8% SDS. Proteins in the samples were then digested with 0.2 mg/ml proteinase K for 2-3 hrs at 37°C, and DNA purified by phenol/chloroform extraction and ethanol precipitation in the presence of 500 mM LiCl and 40 μ g glycogen. Finally, RNA contaminants were removed by treatment with 20 μ g/ml RNase A for 1-2 hrs at 37°C, and samples diluted 5-fold for use as source material in quantification.

To determine the extent of Pho4-specific enrichment, we again employed Q-PCR and fluorescence quantification of SYBR Green I. For each *PHO* promoter, we selected Primer3-designed sequences targeting segments containing Pho4 motifs located in non-nucleosomal regions¹⁴: *PHO5* (-507 → -201), *PHO84* (-457 → -255), *PHO8* (-554 → -344), *PHO89* (-490 → -317), *PHM2* (-385 → -179), *PHM4* (-217 → -26), *PHM6* (-492 → -285). To assess the degree of background enrichment, we selected a primer pair targeting the *POL1* coding sequence: (2497 → 2717). A four point, 8-fold dilution series was prepared from the input DNA of a single arbitrarily-selected sample and used to establish the standard curves specific to each primer set. Again, R^2 values from linear regression exceeded 0.995, and quantification dynamic ranges were consistently large enough to render extrapolation unnecessary. For each P_i condition, we determined *PHO* and *POL1* locus quantities from both Pho4-IP and input samples.

To calculate the fraction of maximal Pho4 enrichment at each of the promoters presented in Fig. 4a, we employed a series of normalizations. For each promoter, quantified values from the IP sample were first normalized to their respective input sample to correct for any culture-specific and chromatin preparation differences. Secondly, each *PHO* promoter ratio was normalized to the *POL1* ratio obtained from the same sample to determine the degree of Pho4-specific enrichment above background. Finally, this signal-to-noise quantity was compared to the same quantity derived from the no P_i sample to calculate the percentage of maximal binding under various induction conditions. For example, Pho4 enrichment at the *PHO5* promoter under intermediate P_i conditions was calculated as follows:

$$\left[\frac{(PHO5 - \text{Int } P_i)_{IP}}{(PHO5 - \text{Int } P_i)_{input}} \right] / \left[\frac{(PHO5 - \text{No } P_i)_{IP}}{(PHO5 - \text{No } P_i)_{input}} \right]$$

$$\left[\frac{(POL1 - \text{Int } P_i)_{IP}}{(POL1 - \text{Int } P_i)_{input}} \right] / \left[\frac{(POL1 - \text{No } P_i)_{IP}}{(POL1 - \text{No } P_i)_{input}} \right]$$

Flow cytometry analysis. Quantification of single-cell fluorescence was performed on an LSR II analytical flow cytometer with 488 nm laser (Becton, Dickinson, and Company, www.bdbiosciences.com). To control for day-to-day instrument variation, a five point calibration sample of fluorescent polystyrene microspheres (Invitrogen #L-14822, www.invitrogen.com) was read at the start and end of each experiment. Signal area data (e.g., FSC-A, FITC-A) for 10,000 cells was collected from all samples and exported in FCS 3.0 format for further post-processing and analysis.

Custom scripts were coded in MATLAB (The Mathworks, www.mathworks.com) and made possible primarily by a function to read the FCS 3.0 format written by Laszlo Balkay (available at the community File Exchange section at www.mathworks.com/matlabcentral). In order to allow for measurement comparisons across experiments and to correct for random sources of electronic variability, a standard curve spanning almost a 1,000 fold dynamic range was established for each experiment by a weighted least-squares fit to the five calibration points. Based on R^2 values that consistently exceeded 0.9999, it is likely instrument linearity extended an additional order of magnitude at both ends. Fluorescence values for samples were interpolated off these standard curves before further analysis. Any reference to “calibrated fluorescence” in this study refer to these standardized units.

Although samples were sonicated before flow cytometry to reduce variability arising from cell aggregation, we performed simple rectangular gating in the forward scatter (FSC) and side scatter (SSC) channels to further reduce variability. We implemented an automated approach whereby data points outside the 0.1 and 0.85 quantiles in either FSC and SSC were eliminated, and this worked well empirically to eliminate debris and any remaining cell aggregates.

Autofluorescence was minimized in all synthetic media experiments by the addition of supplementary adenine and tryptophan. Nevertheless, we included a strain lacking *yeGFP1* in all experiments in order to assess the level of fluorescence specific to gene expression. In lieu of doing subtraction with distribution parameters estimated from the *yeGFP1*⁻ and transcriptional reporter samples, we instead performed a randomly-permuted vector subtraction of autofluorescence from the transcriptional reporter distributions. We deemed this numerical approach as more unbiased as assumptions of normality (i.e., Gaussian) or distribution symmetry would not have to be made. This can be especially important in situations where population behavior is highly skewed (e.g., during induction) or multi-modal.

We took two approaches — “interpolation” and “fit” — to estimate times of half-maximal induction (Supplementary Table S1 and S2). The first is a simple linear interpolation of the time needed to reach a level halfway between the median expression observed at 0 and 7 hrs (Fig. 1c and 2d). Seven hours was chosen as a maximum based on balancing the observations that median expression was changing less than 10% on average and cells were beginning to arrest due to the lack of P_i (resulting in a broadening of the fluorescence distribution).

Because the interpolated half-times are highly dependent on the choice of maximum, we decided to take a second approach for comparison. In the “fit” method, the unscaled kinetic data were subjected to a non-linear least squares fit of a Hill equation with 3 freely varying parameters: n (Hill coefficient), Y_{\max} (asymptotic maximal value), and T_{half} (half maximal time):

$$y = \frac{Y_{\max} t^n}{t^n + T_{\text{half}}^n}$$

where t and y are time points and measured medians, respectively. Because Y_{\max} is now a parameter, T_{half} is not constrained to an arbitrary maximum and free to adopt the value which best approximates the continuous underlying behavior. In general, the fits gave normally distributed residuals centered around zero and low root mean squared errors (fit standard errors), indicating that the Hill model describes the kinetic data well. Additionally, individual 95% confidence intervals can be determined from an analysis of the sensitivities of the parameter estimates to the input data points, and are provided next to each fit-derived T_{half} value. The maximum percentage difference we observe between the two methods throughout all our transcriptional reporter strains is ~30%, suggesting that either approach is suitable for estimating half maximal induction times.

Descriptive statistics and expression variability. In general, the fluorescence distributions we observed from our transcriptional reporter strains were unimodal and highly right-skewed. Transformations of raw calibrated fluorescence data using the logarithm yielded the most symmetric (but not Gaussian) distributions and manageable range.

We generally took the median of the untransformed calibrated fluorescence data as the measure of central tendency (Fig. 1b,c; 2c,d; and Supplementary Fig. S3). To arrive at a proxy for measurement error, we performed steady-state P_i response experiments for the WT and H4 *PHO5* promoter variants in triplicate and observed that the median expression consistently fell well within the interquartile range of the initially measured fluorescence distributions. As a result, error bars in Fig. 1b and 2c indicate interquartile ranges of the calibrated fluorescence distributions measured from a single experiment. We chose to use interquartile range instead of standard deviation because our measured distributions were never lognormal (i.e., did not pass a Lilliefors test for normality³⁰).

For measurements done in replicate with reported error bars (Fig. 3 and Supplementary Fig. S10), the mean of the logged fluorescence values was used. This was done so that we could invoke the central limit theorem and (regardless of the shape of the parent distribution) expect the uncertainty in measurement to be normally distributed. Furthermore, in instances such as Supplementary Fig. S10 where we calculate a quantity based on measured values, the symmetry of the errors allowed us to easily propagate the variability.

Discussions in the text on the range of fractional expression at intermediate P_i conditions generally describe a percentage \pm interval. Because the distributions of the relevant expression levels were never Gaussian or even symmetric, we again reported the median and the interquartile range. For example, the induction values of all the high affinity *PHO5* promoter variants (H1-H4) in intermediate P_i (10, 50, 100 μ M P_i) yields a distribution with a median of 37% and an interquartile spread of 4%. We therefore report this statistic as 37 \pm 2% of maximal induction.

Steady-state expression in response to P_i consistently yielded homogeneous fluorescence populations with low total noise. Supplementary Table S7 lists interquartile ranges in \log_{10} calibrated fluorescence units measured from all transcriptional reporter strains used in this study.

Discussion

Feedback effects. As a secreted acid phosphatase that acts on external organic phosphate sources, *PHO5* was chosen because its absence (i.e., replacement of its coding sequence with yeGFP1), would exhibit no feedback effects in synthetic media. In contrast, the functions of the various *PHO* target genes are not completely characterized and thus, a total deletion (e.g., in a haploid transcriptional reporter) could potentially impair phosphate homeostasis. For example, constitutive *PHO* pathway activation is a known phenotype of *pho84Δ* haploids¹⁰. Therefore, the presence of at least one functional allele in heterozygous diploid transcriptional reporter strains should minimize any perturbation to proper pathway operation.

Resolvability of individual Pho4 sites by ChIP. Chromatin is typically sheared to an average DNA fragment length of 0.5-1 kb before immunoprecipitation with antibodies specific to a transcription factor of interest^{31,32}. Based on fragment size ranges published in the literature^{33,34} (and mean lengths of ~500 bp measured from our samples after sonication (data not shown)) relative to the spacing of Pho4 binding sites in yeast promoters, we were doubtful that binding to individual Pho4 sites could be delineated within the majority of our seven examined *PHO* promoters. However, to experimentally evaluate if this was indeed the case, we attempted to quantify localized Pho4 occupancy by conducting Q-PCR with primer sets (same as those used for mapping nucleosomes) that tile the length of a promoter region.

First, as test cases to determine if distinct Pho4 sites and relative binding affinities can be detected, we mapped the nucleosome-free and nucleosome -2 regions in the promoters of wild-

type *PHO5* and the H4 variant under P_i starvation when both Pho4 sites are known to be fully accessible. Second, to determine if differential binding to the nucleosomal (UASp2) site can be quantified, we mapped the same regions of the two promoters in intermediate (100 μ M) P_i conditions. Consistent with the results in Fig. 4a, we observe a substantial increase in overall Pho4 enrichment between intermediate and no P_i conditions in wild-type *PHO5* (Supplementary Fig. S8a) but less so in the H4 variant (Supplementary Fig. S8b). However, we see from triplicate measurements that the peaks associated with individual Pho4 binding sites within each promoter cannot be statistically separated under either condition.

Resolvability of individual Pho4 sites by ChIP simulation. To supplement our experimental approach, we used computational analysis to explore the resolvability of Pho4 binding sites in the other *PHO* promoters. We developed a simple MATLAB-based simulation of ChIP by modeling the random fragmentation of DNA to any user-definable mean length, followed by the isolation and quantification of fragments containing Pho4 motifs.

In conceptualizing the shearing process, we assumed that the fragmentation points along a stretch of DNA are completely random but constrained only by the number of cuts. For example, given a user-specified mean fragment length of 500 bp, a 10 kb segment of DNA would be randomly cut at 19 points (to produce 20 fragments). This was then repeated 10,000 times (representing 10,000 individual “cells”) for increased statistical power. When the collection of total fragments (200,000, in this example) is analyzed, we found that the histogram of fragment lengths is heavily right-skewed and approximates an exponential distribution (data not shown), consistent with a constant probability of cutting per unit distance of DNA.

We then modeled the process of immunoprecipitation by iterating through each “cell” and examining the set of fragments for the presence of complete Pho4 binding sites; fragments containing no or partial sites were discarded. To quantitatively account for the 13 fold difference in *in vitro* affinity¹⁸, we tested for the presence of low and high affinity sites in a set fraction of the iterations where we tested only for high affinity sites. Specifically, for every iteration in which we searched for high and low affinity sites, we performed 12 iterations in which we searched for high affinity sites only. We adopted this approach for several reasons: 1) it preserves the stochasticity that would otherwise be eliminated had we searched comprehensively for either type of site and discarded a precise fraction of the low affinity hits (e.g., discard 12 low affinity for every 13 high affinity sites), and 2) it eliminates conditions that can arise where fragments containing multiple binding sites in close proximity are counted multiple times.

To model the quantification of immunoprecipitated material, we took our isolated subset of fragments containing Pho4 sites and subjected it to simulated Q-PCR. Using coordinates for primer pairs that tile the length of each *PHO* promoter region (identical to the ones used for mapping nucleosome positions), we examined each DNA fragment to determine if it fully contains each primer set, and if so, a “PCR product” is formed and counted. Formally, we simulate only one round of PCR as that is sufficient to establish the relative steady-state proportion of PCR products. The histogram of tallies along the promoter region was then normalized to the tallest peak and plotted against the center coordinate of each PCR product (again, identical to the approach used for plotting nucleosome positions). Finally, we superimposed onto each point the average experimental error (standard deviation of 3 replicates)

that was observed previously from the promoter Q-PCR measurements of wild-type *PHO5* and the H4 variant.

In Supplementary Fig. S9, we show the results for all seven *PHO* promoters using the Pho4 motifs predicted from PSSM analysis, and under conditions where all sites are accessible or where only non-nucleosomal sites are accessible. Consistent with experimental results (Fig. 4a and Supplementary Fig. S8a), promoters containing an exposed low affinity site (Supplementary Fig. S9a-c) have considerably lower signal in intermediate P_i conditions than in no P_i conditions. In contrast, promoters containing exposed high affinity sites (Supplementary Fig. S9d-g) have substantial Pho4 enrichment in both conditions (unlike real experimental data, however, the intermediate and no P_i traces here overlap because we do not model the increase in nuclear Pho4 activity that occurs between these conditions). Finally, even though we had specified a best-case mean DNA fragment length of 200 bp (likely unattainable with current experimental protocols), we still find that we are unable to distinguish peaks of individual Pho4 binding within the majority of these promoters. We therefore conclude that any differential binding along a promoter region between partially- and fully-activating conditions cannot be resolved with current approaches.

Dynamic range of *PHO* genes. Unlike the promoter threshold of activation where a simple correlation exists between fractional expression at intermediate P_i and affinity of the accessible motif, the determinants of maximum induction appear to be multifactorial and influenced by motif affinity, accessibility, and possibly distance from transcription start. Furthermore, the strength of transcription initiation may be a limiting factor, and as such, the determinants of

dynamic range are likely promoter-specific and not easily generalized among the *PHO* genes. However, for *PHO5* where we have conducted a systematic study of promoter perturbations and which has an efficient TATA box³⁵, it is clear that the impact of nucleosomal sites on gene expression is not evident until after the threshold has been surpassed and the promoter is activated.

Prediction of expression in YPD. As further experimental validation of the promoter architectural principles uncovered in this study, we wanted to assess our predictions for the magnitude of expression in YPD, a rich media and standard laboratory growth condition. Although abundant in organic phosphate sources, YPD is known to be limiting for P_i and capable of promoting an intermediate *PHO* response³⁶. We therefore expected *PHO84*, *PHO8*, *PHM2*, and *PHM4* to induce substantially, and *PHO5*, *PHO89*, and *PHM6* to remain mostly down-regulated. Accessing the maximal promoter state physiologically with YPD is problematic due to its non-synthetic nature. We therefore created strains homozygously deleted for the *PHO80* gene, which results in a constitutively-activated *PHO* pathway and provides the maximum expression levels needed for data normalization. When the steady-state expression levels of the diploid transcriptional reporter and derivative *pho80*Δ strains grown in YPD are measured and compared, we observe that the high affinity class is, in fact, induced to between 37-58% of maximum while the low affinity class to between 7-14% (Supplementary Fig. S10).

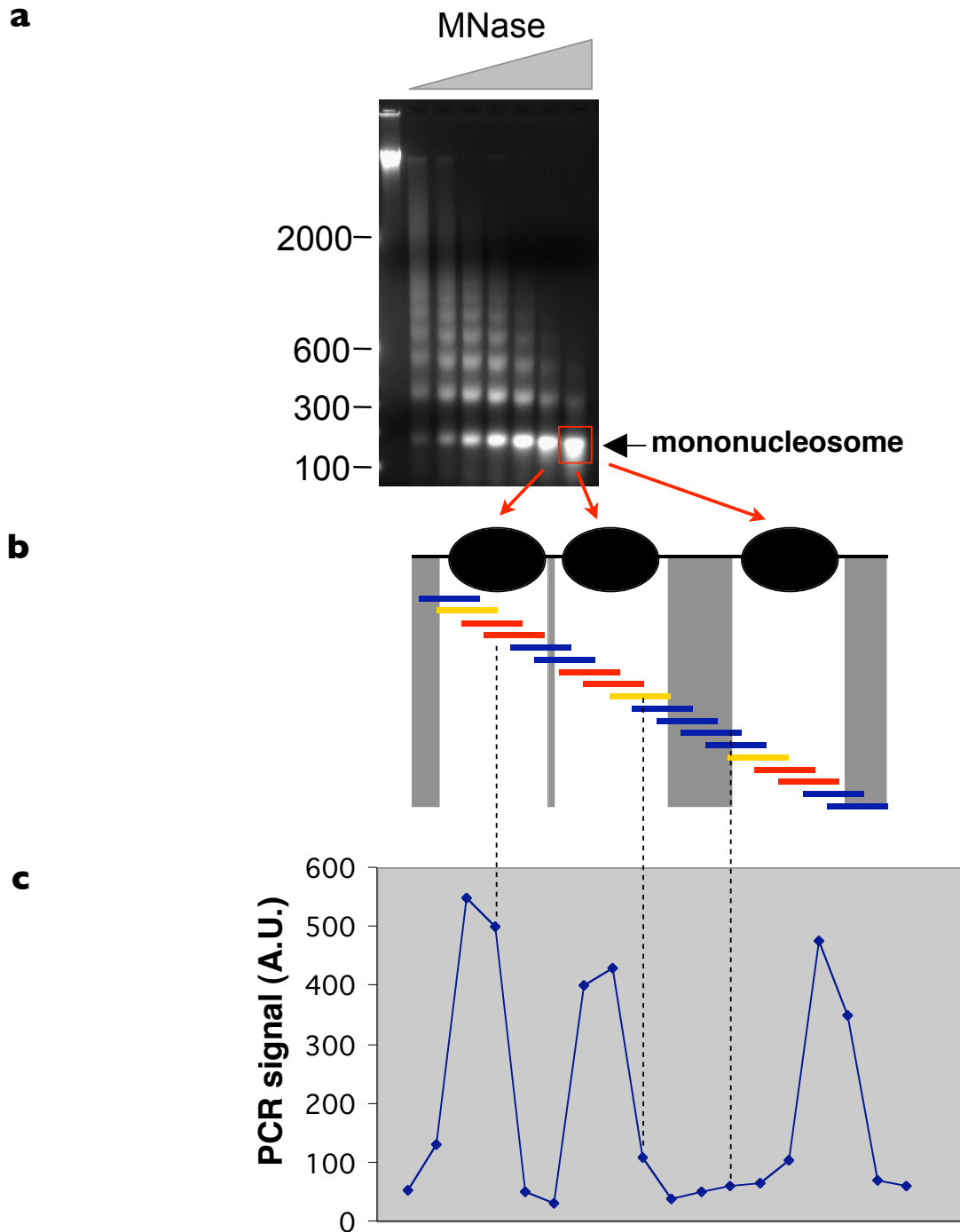
References

1. Guthrie, C. & Fink, G.R. *Guide to yeast genetics and molecular biology*, (Academic Press, San Diego, 1991).
2. Ausubel, F.M. *Current protocols in molecular biology*. (J. Wiley, New York, 1987).
3. Sikorski, R.S. & Hieter, P. A system of shuttle vectors and yeast host strains designed for efficient manipulation of DNA in *Saccharomyces cerevisiae*. *Genetics* **122**, 19-27 (1989).
4. Cormack, B.P., *et al.* Yeast-enhanced green fluorescent protein (yEGFP) a reporter of gene expression in *Candida albicans*. *Microbiology* **143 (Pt 2)**, 303-311 (1997).
5. Longtine, M.S., *et al.* Additional modules for versatile and economical PCR-based gene deletion and modification in *Saccharomyces cerevisiae*. *Yeast* **14**, 953-961 (1998).
6. Miyasaka, H. The positive relationship between codon usage bias and translation initiation AUG context in *Saccharomyces cerevisiae*. *Yeast* **15**, 633-637 (1999).
7. Kaffman, A., Herskowitz, I., Tjian, R. & O'Shea, E.K. Phosphorylation of the transcription factor PHO4 by a cyclin-CDK complex, PHO80-PHO85. *Science* **263**, 1153-1156 (1994).
8. Thomas, M.R. & O'Shea, E.K. An intracellular phosphate buffer filters transient fluctuations in extracellular phosphate levels. *Proc Natl Acad Sci U S A* **102**, 9565-9570 (2005).
9. *Difco & BBL Manual, Manual of Microbiological Culture Media*, (Diagnostic Systems, Sparks, MD).
10. Wykoff, D.D. & O'Shea, E.K. Phosphate transport and sensing in *Saccharomyces cerevisiae*. *Genetics* **159**, 1491-1499 (2001).
11. Sekinger, E.A., Moqtaderi, Z. & Struhl, K. Intrinsic histone-DNA interactions and low nucleosome density are important for preferential accessibility of promoter regions in yeast. *Mol Cell* **18**, 735-748 (2005).
12. Bouchard, C., *et al.* Regulation of cyclin D2 gene expression by the Myc/Max/Mad network: Myc-dependent TRRAP recruitment and histone acetylation at the cyclin D2 promoter. *Genes Dev* **15**, 2042-2047 (2001).
13. Morrison, A.J., Sardet, C. & Herrera, R.E. Retinoblastoma protein transcriptional repression through histone deacetylation of a single nucleosome. *Mol Cell Biol* **22**, 856-865 (2002).
14. Rozen, S. & Skaletsky, H. Primer3 on the WWW for general users and for biologist programmers. *Methods Mol Biol* **132**, 365-386 (2000).
15. Jessen, W.J., Hoose, S.A., Kilgore, J.A. & Kladde, M.P. Active PHO5 chromatin encompasses variable numbers of nucleosomes at individual promoters. *Nat Struct Mol Biol* **13**, 256-263 (2006).
16. Ogawa, N., DeRisi, J. & Brown, P.O. New components of a system for phosphate accumulation and polyphosphate metabolism in *Saccharomyces cerevisiae* revealed by genomic expression analysis. *Mol Biol Cell* **11**, 4309-4321 (2000).
17. Ogawa, N., Hayashi, N., Saito, H., Noguchi, K. & Yamashita, Y. Regulatory circuit for phosphatase genes in *Saccharomyces cerevisiae*: specific *cis*-acting sites in *PHO* promoters for binding the positive regulator Pho4p. in *Phosphate in Microorganisms*:

- Cellular and Molecular Biology* (eds. Torriani-Gorini, A., Yagil, E. & Silver, S.) 56-62 (American Society for Microbiology, Washington, D.C., 1994).
18. Maerkl, S.J. & Quake, S.R. A systems approach to measuring the binding energy landscapes of transcription factors. *Science* **315**, 233-237 (2007).
 19. Shimizu, T., *et al.* Crystal structure of PHO4 bHLH domain-DNA complex: flanking base recognition. *Embo J* **16**, 4689-4697 (1997).
 20. GuhaThakurta, D. Computational identification of transcriptional regulatory elements in DNA sequence. *Nucleic Acids Res* **34**, 3585-3598 (2006).
 21. Barbaric, S., Fascher, K.D. & Horz, W. Activation of the weakly regulated PHO8 promoter in *S. cerevisiae*: chromatin transition and binding sites for the positive regulatory protein PHO4. *Nucleic Acids Res* **20**, 1031-1038 (1992).
 22. Venter, U., Svaren, J., Schmitz, J., Schmid, A. & Horz, W. A nucleosome precludes binding of the transcription factor Pho4 in vivo to a critical target site in the PHO5 promoter. *Embo J* **13**, 4848-4855 (1994).
 23. Ogawa, N., *et al.* Structure and distribution of specific cis-elements for transcriptional regulation of PHO84 in *Saccharomyces cerevisiae*. *Mol Gen Genet* **249**, 406-416 (1995).
 24. Munsterkotter, M., Barbaric, S. & Horz, W. Transcriptional regulation of the yeast PHO8 promoter in comparison to the coregulated PHO5 promoter. *J Biol Chem* **275**, 22678-22685 (2000).
 25. Kellis, M., Patterson, N., Endrizzi, M., Birren, B. & Lander, E.S. Sequencing and comparison of yeast species to identify genes and regulatory elements. *Nature* **423**, 241-254 (2003).
 26. Kent, W.J., *et al.* The human genome browser at UCSC. *Genome Res* **12**, 996-1006 (2002).
 27. Magbanua, J.P., Fujisawa, K., Ogawa, N. & Oshima, Y. The homeodomain protein Pho2p binds at an A/T-rich segment flanking the binding site of the basic-helix-loop-helix protein Pho4p in the yeast PHO promoters. *Yeast* **13**, 1299-1308 (1997).
 28. Hecht, A. & Grunstein, M. Mapping DNA interaction sites of chromosomal proteins using immunoprecipitation and polymerase chain reaction. *Methods in enzymology* **304**, 399-414 (1999).
 29. Springer, M., Wykoff, D.D., Miller, N. & O'Shea, E.K. Partially phosphorylated Pho4 activates transcription of a subset of phosphate-responsive genes. *PLoS Biol* **1**, E28 (2003).
 30. Lilliefors, H.W. On the Komogorov-Smirnov test for normality with mean and variance unknown. *Journal of the American Statistical Association* **62**, 399-402 (1967).
 31. Aparicio, O.M., *et al.* Chromatin Immunoprecipitation for Determining the Association of Proteins with Specific Genomic Sequences In Vivo. in *Current Protocols in Molecular Biology* (eds. Ausubel, F.M., *et al.*) (John Wiley & Sons, Inc., New York, 2005).
 32. Orlando, V. Mapping chromosomal proteins in vivo by formaldehyde-crosslinked-chromatin immunoprecipitation. *Trends in biochemical sciences* **25**, 99-104 (2000).
 33. Strahl-Bolsinger, S., Hecht, A., Luo, K. & Grunstein, M. SIR2 and SIR4 interactions differ in core and extended telomeric heterochromatin in yeast. *Genes Dev* **11**, 83-93 (1997).

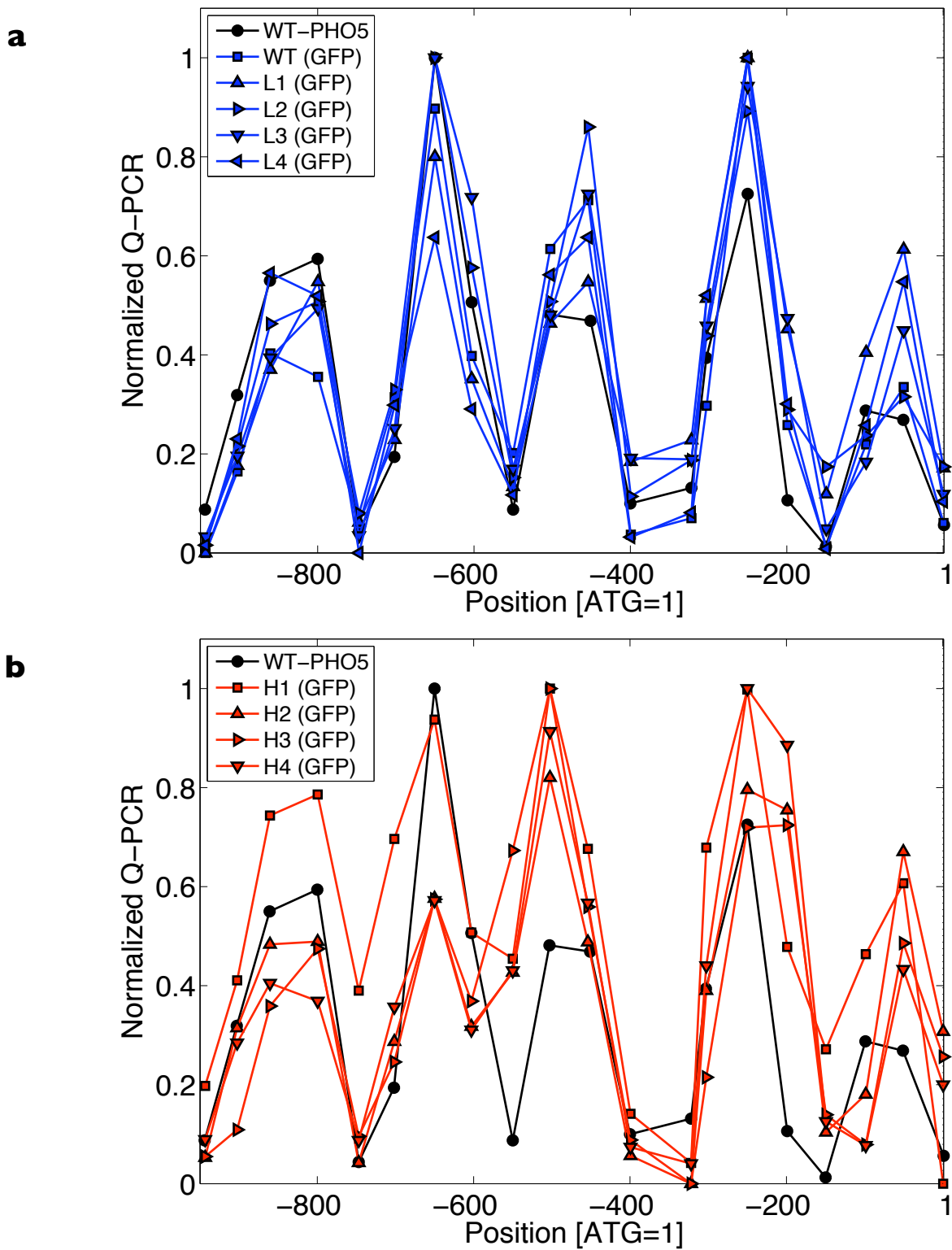
34. Ren, B., *et al.* Genome-wide location and function of DNA binding proteins. *Science* **290**, 2306-2309 (2000).
35. Raser, J.M. & O'Shea, E.K. Control of stochasticity in eukaryotic gene expression. *Science* **304**, 1811-1814 (2004).
36. Neef, D.W. & Kladde, M.P. Polyphosphate loss promotes SNF/SWI- and Gcn5-dependent mitotic induction of PHO5. *Mol Cell Biol* **23**, 3788-3797 (2003).

Supplementary Figure S1



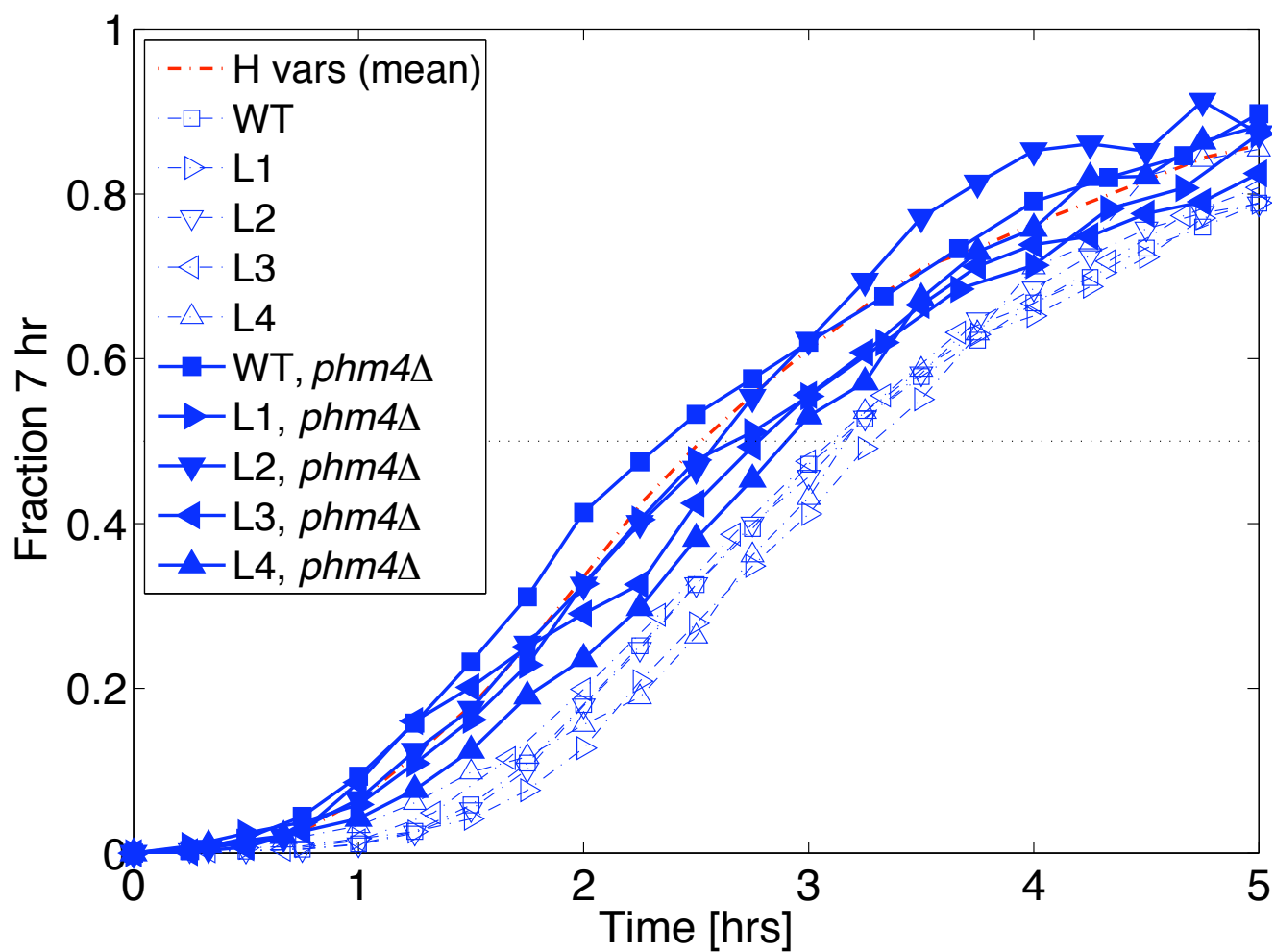
Supplementary Figure S1. Summary of nucleosome mapping technique. **a**, Spheroplasts are treated with increasing amounts of micrococcal nuclease (MNase), DNA is purified, and mononucleosome-length fragments are gel-isolated. **b**, Mononucleosome-length DNA is used as template in Q-PCR with overlapping primer pairs that tile the length of a promoter. **c**, Promoter regions completely protected from MNase digestion by nucleosomes will result in high PCR signal (red primer pairs in **b**), partial protection in intermediate PCR signal (yellow primer pairs), and no protection in minimal PCR signal (blue primer pairs). See Materials and Methods > Nucleosome maps for details.

Supplementary Figure S2



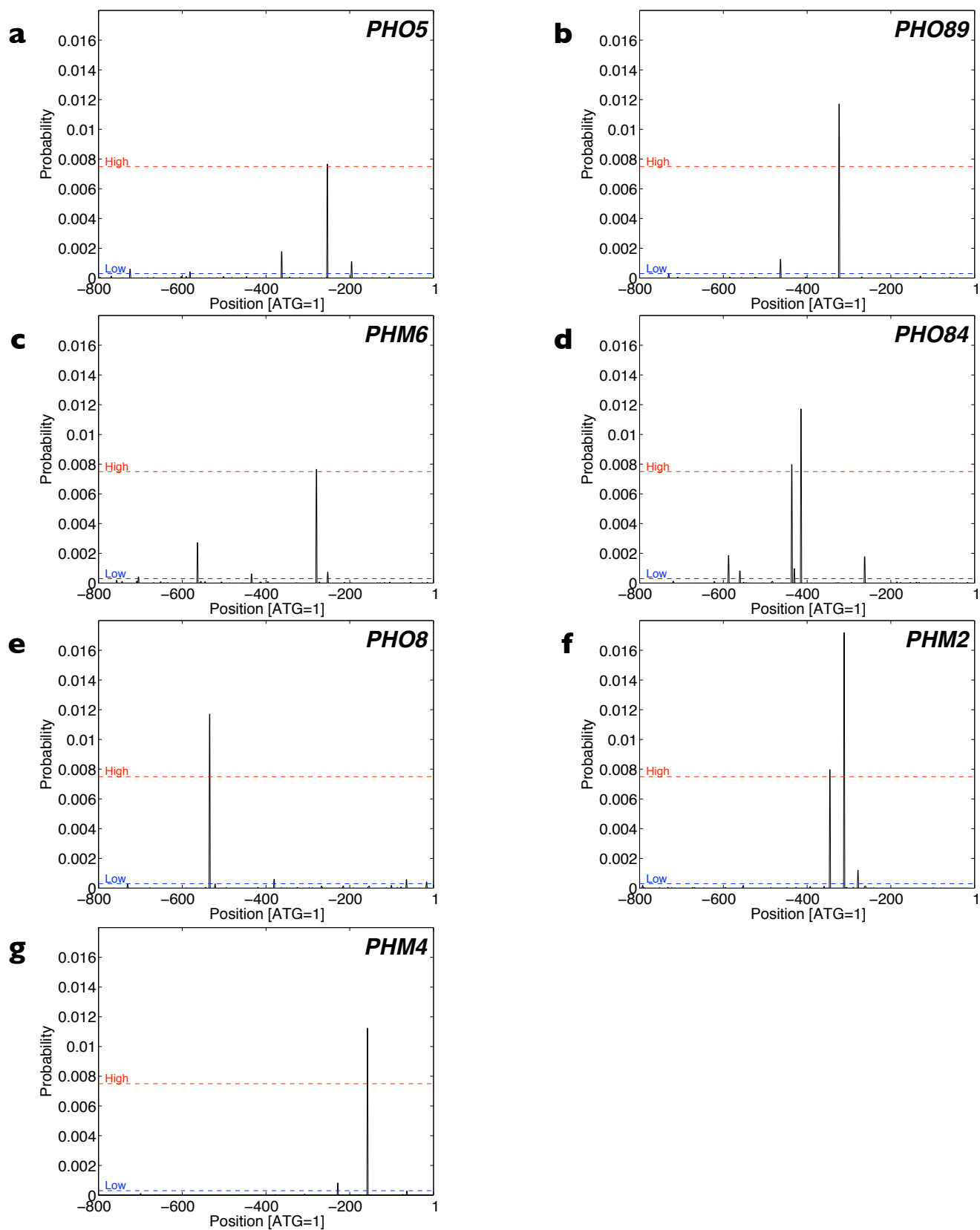
Supplementary Figure S2. Promoter nucleosome positions are minimally impacted by mutations creating the *PHO5* promoter variants or by the presence of the yeGFP1 coding sequence. For reference, the chromatin map of the wild-type *PHO5* promoter with native *PHO5* protein coding sequence is included in black on both plots. Nucleosome maps for the *PHO5* promoter variants were all measured in 10 mM P_i from transcriptional reporter strains containing yeGFP1 (see Supplementary Table S4). **a**, Variants with exposed low affinity Pho4 binding site (L1-L4). **b**, Variants with exposed high affinity Pho4 binding site (H1-H4).

Supplementary Figure S3



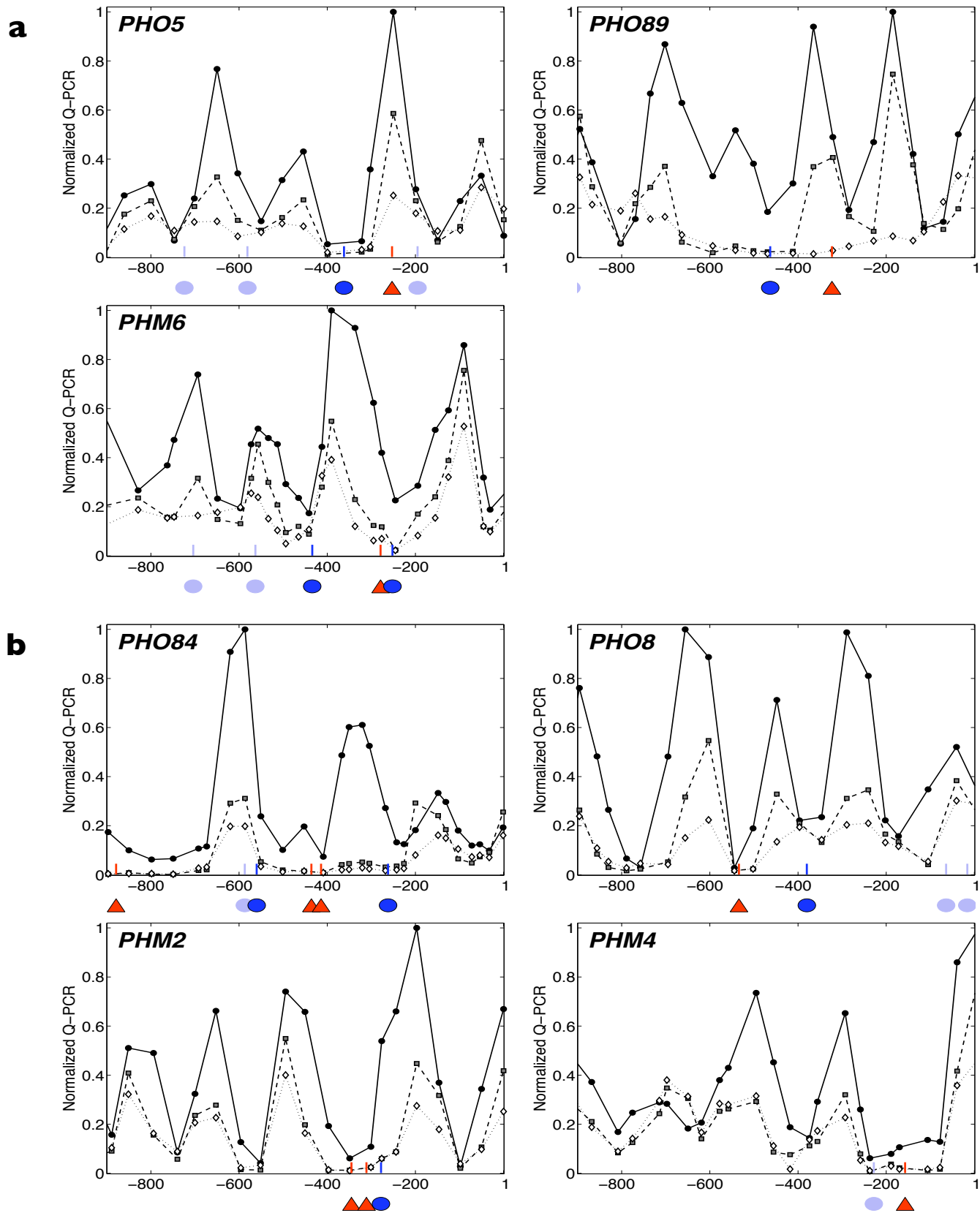
Supplementary Figure S3. The kinetic difference observed during no P_i induction between exposed high (H vars, mean) and low affinity (WT; L1-L4) *PHO5* promoter variants is largely mitigated by deletion of *PHM4* (dark blue traces – WT, *phm4*Δ; L1-L4, *phm4*Δ). See Supplementary Table S1 for half-maximal times. Each point represents the time-dependent median expression scaled between the repressed state at 0 hr and the median measured at 7 hr.

Supplementary Figure S4



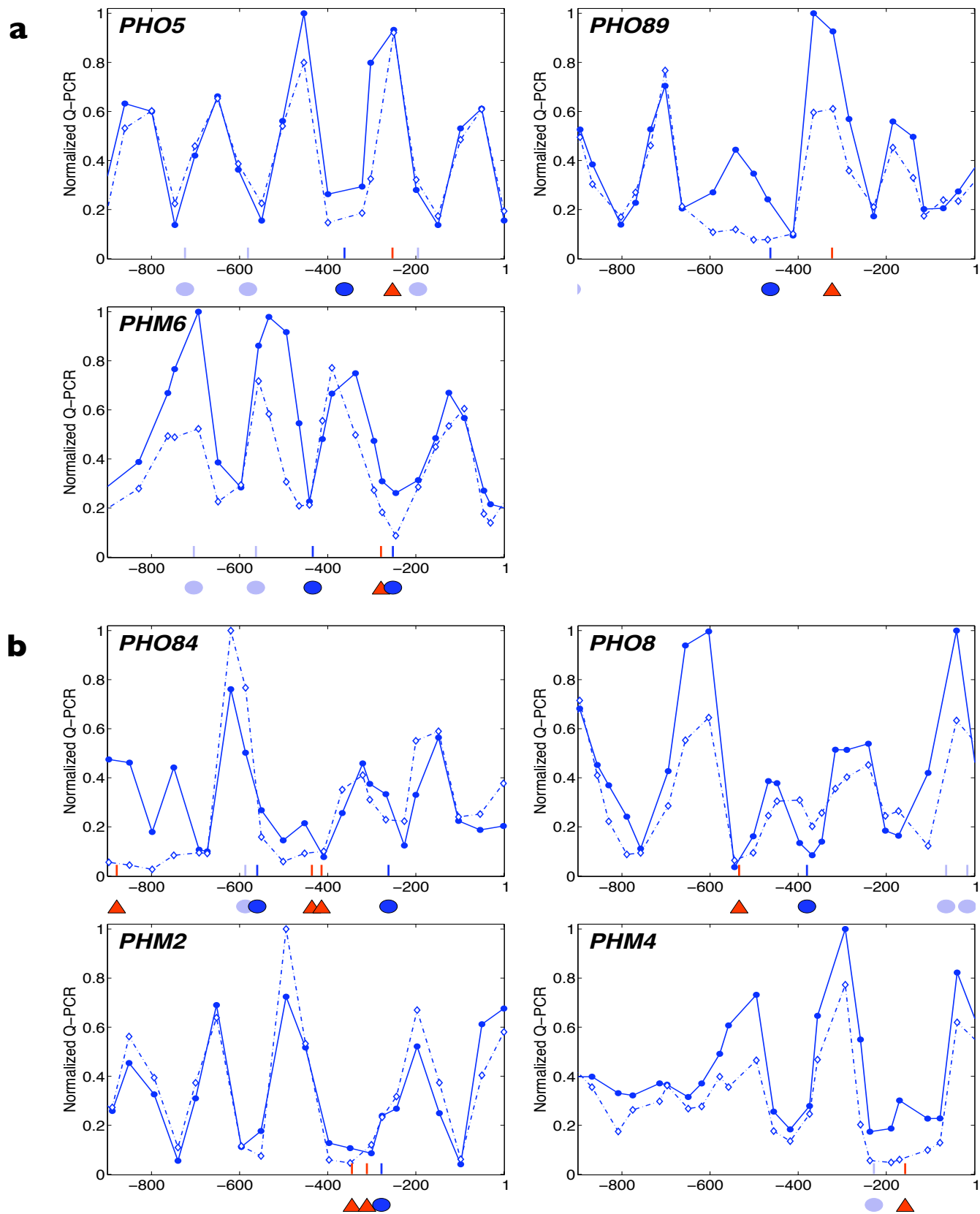
Supplementary Figure S4. Pho4 promoter binding profiles from position-specific scoring matrix (PSSM) analysis of **a**, *PHO5*; **b**, *PHO89*; **c**, *PHM6*; **d**, *PHO84*; **e**, *PHO8*; **f**, *PHM2/VTC3*; and **g**, *PHM4/VTC1*. The blue dashed line (“Low”) on each plot designates the probability noise threshold (3×10^{-4}) chosen for likely Pho4 regulatory elements. Motifs scoring above 0.0075 (red dashed line, “High”) are considered high affinity while those between 3×10^{-4} and 0.0075 are considered low affinity.

Supplementary Figure S6



Supplementary Figure S6. Promoter chromatin maps of *PHO* target genes assayed from wild-type cells in 10 mM (solid black circles; reprinted from Fig. 2a, b), 100 μ M (dashed gray squares), and 0 μ M P_i (dotted white diamonds). Pho4 motifs (blue ovals and red triangles) are the same as in Fig. 2a,b, and x axis units reference promoter coordinates where ATG=1. **a**, *PHO* promoters with an accessible low affinity Pho4 binding site. **b**, *PHO* promoters with at least one accessible high affinity Pho4 binding site.

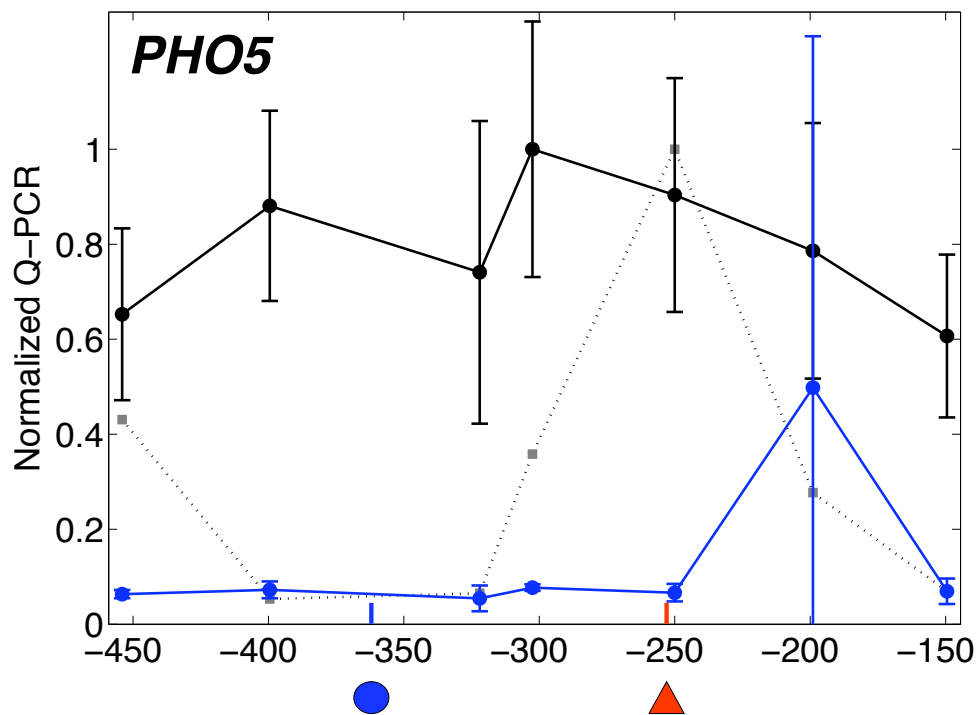
Supplementary Figure S7



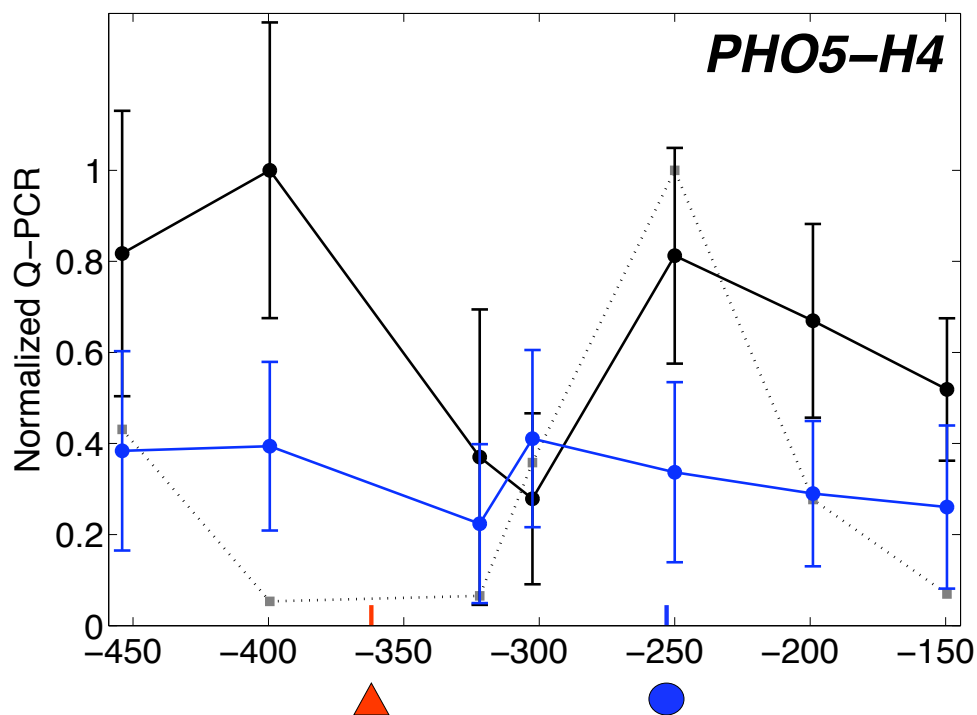
Supplementary Figure S7. Promoter chromatin maps of *PHO* target genes assayed from *pho2Δ* cells in 10 mM (solid blue circles) and 0 mM P_i (dotted white diamonds). Pho4 motifs (blue ovals and red triangles) are the same as in Fig. 2a,b, and *x* axis units reference promoter coordinates where ATG=1. **a**, *PHO* promoters with an accessible low affinity Pho4 binding site. **b**, *PHO* promoters with at least one accessible high affinity Pho4 binding site.

Supplementary Figure S8

a

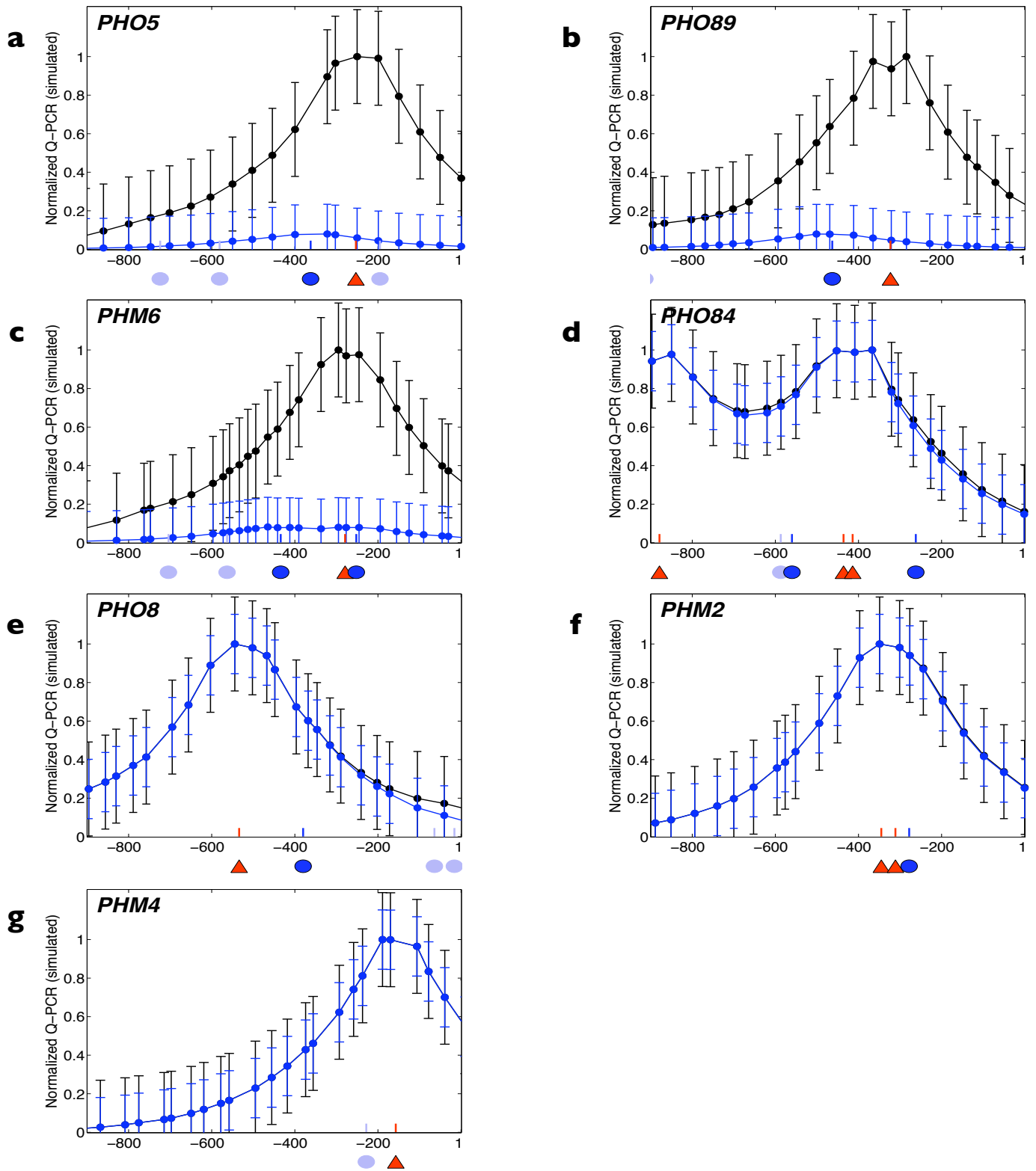


b



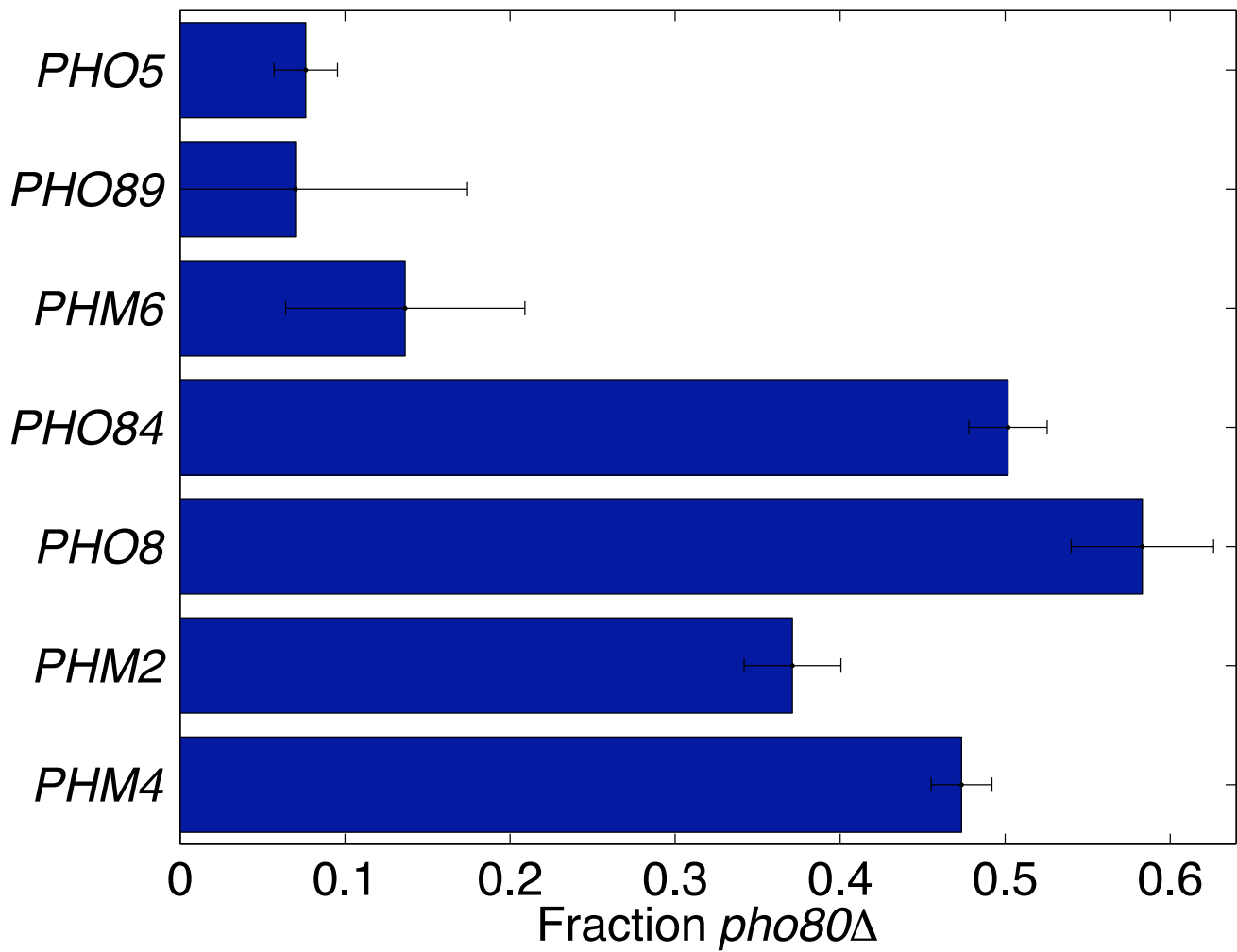
Supplementary Figure S8. Chromatin immunoprecipitation of Pho4 followed by Q-PCR using primer pairs tiling across the nucleosome-free and nucleosome -2 regions in the promoters of wild-type *PHO5* (a) and the H4 variant (b). Cells were grown in intermediate (100 μM , blue trace) or no (0 μM , black trace) P_i medium for 2.5 hrs, and the ratio of Pho4 enrichment at each promoter coordinate over *POL1* was measured and further re-normalized to the maximum mean observed. Error bars are standard deviations from 3 independent experiments. For reference, the dotted trace represents nucleosome positions under repressive conditions, red triangles are high affinity Pho4 motifs, blue ovals low affinity Pho4 motifs, and x axis units reference promoter coordinates where ATG=1.

Supplementary Figure S9




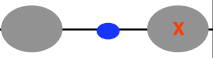

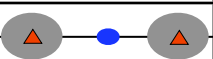
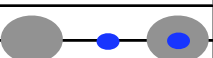
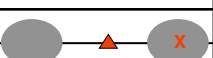
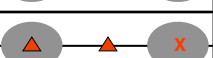


Supplementary Figure S9. Simulations of Pho4 chromatin immunoprecipitation and promoter tiling Q-PCR of **a**, *PHO5*; **b**, *PHO89*; **c**, *PHM6*; **d**, *PHO84*; **e**, *PHO8*; **f**, *PHM2/VTC3*; and **g**, *PHM4/VTC1*. Black traces depict simulation results from a scenario where all Pho4 sites are exposed, and blue traces from a scenario where only non-nucleosomal sites are exposed. Simulations were run using a mean DNA fragment length of 200 bp and a 13 fold difference in K_d between high and low affinity binding sites. Error bars are the average standard deviation superimposed from triplicate promoter ChIP measurements of wild-type *PHO5* and the H4 variant in intermediate or no P_i conditions (Supplementary Figure S8). Red triangles are high affinity Pho4 motifs, blue ovals are low affinity Pho4 motifs, and x axis units reference promoter coordinates where ATG=1.

Supplementary Figure S10



Supplementary Figure S10. Promoter architectural principles correctly estimate the fraction of maximal expression in YPD. The steady-state expression of heterozygous transcriptional reporter strains and derivative strains in a homozygous *pho80*Δ genetic background were measured and a ratio of their means taken. Error bars represent the propagated standard error from separate triplicate measurements of reporter and *pho80*Δ strains.

Supplementary Table S1. Times for half maximal expression in all *PHO5* promoter variants (left half of table; from Fig. 1c), and exposed low-affinity *PHO5* promoter variants (WT, L1-L4) harboring a deletion of *PHM4* (right half of table; from Supplementary Fig. S3) when transferred from 10 mM to 0 mM P_i medium. Values were determined via two methods (“interpolation” and “fit”) for comparison — see Material and Methods > Flow cytometry analysis for description. A 95% confidence interval derived from fitting statistics is provided for each fit value. Table cell colors reflect an exposed low (blue) or high (red) affinity Pho4 binding site.

| | | Interpolation [hrs] | Fit [hrs] | Interpolation, <i>phm4Δ</i> [hrs] | Fit, <i>phm4Δ</i> [hrs] |
|----|---|---------------------|-------------|-----------------------------------|-------------------------|
| WT |  | 3.13 | 3.35 ± 0.17 | 2.36 | 2.66 ± 0.12 |
| L1 |  | 3.29 | 3.52 ± 0.13 | 2.67 | 2.98 ± 0.16 |
| L2 |  | 3.15 | 3.25 ± 0.13 | 2.60 | 2.58 ± 0.09 |
| L3 |  | 3.10 | 3.42 ± 0.17 | 2.78 | 3.10 ± 0.22 |
| L4 |  | 3.16 | 3.39 ± 0.11 | 2.90 | 3.02 ± 0.08 |
| H1 |  | 2.44 | 2.55 ± 0.09 | — | — |
| H2 |  | 2.54 | 2.64 ± 0.08 | — | — |
| H3 |  | 2.62 | 3.08 ± 0.24 | — | — |
| H4 |  | 2.53 | 2.59 ± 0.07 | — | — |

Supplementary Table S2. Times for half maximal expression in heterozygous transcriptional reporter strains when transferred from 10 mM to 0 mM P_i medium (from Fig. 2d). See Material and Methods > Flow cytometry analysis for explanation of “interpolation” and “fit” methods. A 95% confidence interval derived from fitting statistics is provided for each fit value. Table cell colors reflect an exposed low (blue) or high (red) affinity Pho4 binding site.

| | Interpolation [hrs] | Fit [hrs] |
|--------------|----------------------------|------------------|
| <i>PHO5</i> | 3.30 | 4.01 ± 0.28 |
| <i>PHO89</i> | 3.29 | 4.40 ± 0.47 |
| <i>PHM6</i> | 3.69 | 4.80 ± 0.33 |
| <i>PHO84</i> | 2.60 | 3.75 ± 0.48 |
| <i>PHO8</i> | 2.39 | 3.16 ± 0.38 |
| <i>PHM2</i> | 2.02 | 2.32 ± 0.15 |
| <i>PHM4</i> | 2.02 | 2.31 ± 0.21 |

Supplementary Table S3. Promoter dynamic ranges. List of minimum and maximum expression values (lowest and highest distribution medians observed from 50 mM and 0 mM P_i, respectively, in calibrated fluorescence units) for each strain whose physiological response profile was measured. *PHO5* promoter variants are listed in the top set (from Fig. 1b); *PHO* target genes in the bottom set (from Fig. 2c). For experiments done in replicate, an average median is reported. Colors reflect an exposed low (blue) or high (red) affinity Pho4 binding site.

| Strain | Min [calib. fluor.] | Max [calib. fluor.] |
|-----------------------|---------------------|---------------------|
| EY1903 / WT | 0.92 | 83.35 |
| EY1907 / L1 | 1.04 | 20.99 |
| EY1929 / L2 | 0.92 | 60.21 |
| EY1948 / L3 | 0.82 | 149.21 |
| EY2395 / L4 | 1.09 | 20.01 |
| EY1910 / H1 | 1.06 | 52.15 |
| EY1933 / H2 | 1.05 | 85.99 |
| EY1922 / H3 | 1.13 | 102.47 |
| EY1926 / H4 | 0.86 | 56.33 |
| EY2192 / <i>PHO5</i> | 0.72 | 116.37 |
| EY2196 / <i>PHO89</i> | 0.21 | 42.76 |
| EY2204 / <i>PHM6</i> | 0.37 | 43.92 |
| EY2230 / <i>PHO84</i> | 0.99 | 124.31 |
| EY2200 / <i>PHO8</i> | 2.43 | 17.59 |
| EY2198 / <i>PHM2</i> | 1.15 | 33.59 |
| EY2202 / <i>PHM4</i> | 4.41 | 46.15 |

Supplementary Table S4. Haploid *PHO5* promoter variant transcriptional reporter strains used in this study. All strains derived from EY57 (K699 *MATa ade2-1 trp1-1 can1-100 leu2-3,112 his3-11,15 ura3*). *Cg*, *Candida glabrata*; *yeGFP1*, yeast-enhanced green fluorescent protein; and *Kan*, *E. coli kan^r* (resistance to G418). Table cell colors reflect an exposed low affinity (blue) or exposed high affinity (red) Pho4 binding site.

| | | <i>pho5Δ::yeGFP1-Kan</i> | <i>pho5Δ::yeGFP1-Kan</i> , <i>pho80Δ::CgHIS3</i> | <i>pho5Δ::yeGFP1-Kan</i> , <i>phm4Δ::CgLEU2</i> |
|----|--|--------------------------|---|--|
| WT | | EY1903 | EY1905 | EY2157 |
| L1 | | EY1907 | EY1908 | EY2158 |
| L2 | | EY1929 | EY1931 | EY2162 |
| L3 | | EY1948 | EY1949 | EY2164 |
| L4 | | EY2395 | EY2399 | EY2405 |
| H1 | | EY1910 | EY1912 | — |
| H2 | | EY1933 | EY1935 | — |
| H3 | | EY1922 | EY1924 | — |
| H4 | | EY1926 | EY1927 | — |

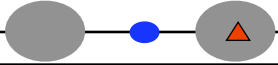
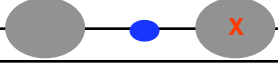
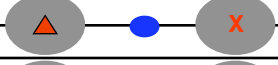
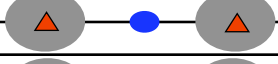
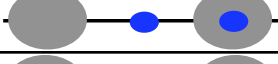
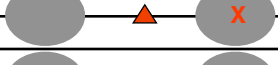
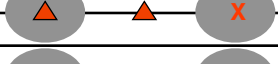


Supplementary Table S5. Heterozygous diploid *PHO* promoter transcriptional reporter strains used in this study. All strains derived from EY2176 (K699 *MATa/α ade2-1/ade2-1 trp1-1/trp1-1 can1-100/can1-100 leu2-3,112/leu2-3,112 his3-11,15/his3-11,15 ura3/ura3*) or EY2177 (K699 *MATa/α ade2-1/ade2-1 trp1-1/trp1-1 can1-100/can1-100 leu2-3,112/leu2-3,112 his3-11,15/his3-11,15 ura3/ura3 pho80Δ::CgHIS3/pho80Δ::CgHIS3*).

| Strain | Genotype |
|---------------|---|
| EY2192 | <i>PHO5/pho5Δ::yeGFP1-Kan</i> |
| EY2193 | <i>PHO5/pho5Δ::yeGFP1-Kan pho80Δ::CgHIS3/pho80Δ::CgHIS3</i> |
| EY2196 | <i>PHO89/pho89Δ::yeGFP1-Kan</i> |
| EY2197 | <i>PHO89/pho89Δ::yeGFP1-Kan pho80Δ::CgHIS3/pho80Δ::CgHIS3</i> |
| EY2198 | <i>PHM2/phm2Δ::yeGFP1-Kan</i> |
| EY2199 | <i>PHM2/phm2Δ::yeGFP1-Kan pho80Δ::CgHIS3/pho80Δ::CgHIS3</i> |
| EY2200 | <i>PHO8/pho8Δ::yeGFP1-Kan</i> |
| EY2201 | <i>PHO8/pho8Δ::yeGFP1-Kan pho80Δ::CgHIS3/pho80Δ::CgHIS3</i> |
| EY2202 | <i>PHM4/phm4Δ::yeGFP1-Kan</i> |
| EY2203 | <i>PHM4/phm4Δ::yeGFP1-Kan pho80Δ::CgHIS3/pho80Δ::CgHIS3</i> |
| EY2204 | <i>PHM6/phm6Δ::yeGFP1-Kan</i> |
| EY2205 | <i>PHM6/phm6Δ::yeGFP1-Kan pho80Δ::CgHIS3/pho80Δ::CgHIS3</i> |
| EY2230 | <i>PHO84/PHO84 ura3/ura3::PHO84pr-yeGFP1-URA3</i> |
| EY2231 | <i>PHO84/PHO84 ura3/ura3::PHO84pr-yeGFP1-URA3 pho80Δ::CgHIS3/pho80Δ::CgHIS3</i> |

Supplementary Table S6. PCR primer sequences used with plasmid template EB1632 for generating gene-specific yeGFP1-kanMX6 targeting cassettes.

| Primer | Sequence |
|---------------|---|
| PHO5-GFPf | agaacaacaacaaatagagcaagcaaattcgagattaccaacctgtctaaaggtgaaga |
| PHO5-GFPr | tattcgtatTTtagTTTccaatattatTTtagTTatacaaaaagaattcgagctcgTTTaaac |
| PHO89-GFPf | cgtatctaatacgaatcaatataaaacaaagattaagcaaaaacctgtctaaaggtgaaga |
| PHO89-GFPr | aatgTTgtaaaactgtattcataaccgaaacacattatgagaattcgagctcgTTTaaac |
| PHM6-GFPf | aaaaaaaaacgacagcaattgTTTTTcaacctgacaccaagacctgtctaaaggtgaaga |
| PHM6-GFPr | gaaaaatcTTgaaagaaaacaaatcccattattcTTtattagaattcgagctcgTTTaaac |
| PHO84-GFPf | cagggcacacaacaaacaaaactccacgaatacaatccaaacctgtctaaaggtgaaga |
| PHO84-GFPr | TTTgTTctagTTTtacaagTTTTtagTgcatcTTTgaggcTTgaaattcgagctcgTTTaaac |
| PHO8-GFPf | tatcagcatacgggacattatttgaacgcgcatttagcagcaccatgtctaaaggtgaaga |
| PHO8-GFPr | attaaataatatgtgaaaaagaggggagagTTtagataggagaattcgagctcgTTTaaac |
| PHM2-GFPf | gcgaacagcagaattTTgtcCTTggTTTTcagagTTTgaaaacctgtctaaaggtgaaga |
| PHM2-GFPr | actTgtgtaatatatgtgtatataaaaaatatacatgTTcgaattcgagctcgTTTaaac |
| PHM4-GFPf | ttatcgaatacgattaaacactacgccagattTccacaataacctgtctaaaggtgaaga |
| PHM4-GFPr | TTTgtgcgtaaccacgctTtacgatattggaattacaattgaaattcgagctcgTTTaaac |

Supplementary Table S7. Variability in steady-state expression observed in the *PHO5* promoter variants (haploid transcriptional reporters) and *PHO* target genes (diploid heterozygous transcriptional reporters). Fluorescence data in calibrated fluorescence units were transformed (\log_{10}) and the interquartile range (IQR) of the resulting distribution reported. For each P_i range (no, intermediate, high), the smallest and largest IQR are listed. All distributions were unimodal. Colors reflect an exposed low (blue) or high (red) affinity Pho4 binding site.

| | Interquartile range [\log_{10} calib. fluor.] | | |
|---|--|-------------------------|---------------------|
| | No (0 μ M) | Int (10-100 μ M) | High (0.5-50 mM) |
|  | 0.305 | 0.420 – 0.444 | 0.384 – 0.463 |
|  | 0.352 | 0.303 – 0.305 | 0.276 – 0.337 |
|  | 0.288 | 0.376 – 0.384 | 0.343 – 0.362 |
|  | 0.214 | 0.378 – 0.392 | 0.402 – 0.438 |
|  | 0.230 | 0.281 – 0.302 | 0.237 – 0.259 |
|  | 0.288 | 0.227 – 0.237 | 0.357 – 0.381 |
|  | 0.268 | 0.199 – 0.202 | 0.332 – 0.358 |
|  | 0.146 | 0.165 – 0.169 | 0.367 – 0.382 |
|  | 0.238 | 0.227 – 0.234 | 0.418 – 0.435 |
| <i>PHO5</i> | 0.323 | 0.400 – 0.430 | 0.445 – 0.461 |
| <i>PHO89</i> | 0.351 | 0.484 – 0.512 | 0.514 – 0.540 |
| <i>PHM6</i> | 0.230 | 0.375 – 0.383 | 0.503 – 0.547 |
| <i>PHO84</i> | 0.144 | 0.171 – 0.173 | 0.342 – 0.361 |
| <i>PHO8</i> | 0.241 | 0.230 – 0.232 | 0.322 – 0.327 |
| <i>PHM2</i> | 0.282 | 0.177 – 0.180 | 0.354 – 0.383 |
| <i>PHM4</i> | 0.264 | 0.178 – 0.188 | 0.222 – 0.242 |